ELSEVIER

Critical Flow in Convergent–Divergent Nozzles with Cavity Nucleation Model

J. L. Xu
Institute of Nuclear Energy Technology, Tsinghua University, Beijing, 100084, People's Republic of China

T. K. Chen

X. J. Chen
National Lab. on Multiphase Flow in Power Engineering, Xi'an Jiaotong University, Xi'an, Shaanxi Province, 710049, People's Republic of China

■ A transient critical flow experiment with convergent–divergent nozzle as the break geometry was conducted in the high-pressure steam–water test loop of Xian Jiaotong University. The test parameters were pressure 3.0–16.0 MPa, inlet liquid stagnation subcooling 0–60°C, and corresponding critical mass flow rate (40–120) × 10^3 kg/(m^2 s). The concept of the incipient flashing, with the choking plane occurring at the throat location, was applied in a wall surface cavity nucleation model. The total pressure difference between the inlet pressure P_0 and the pressure at the throat location P_t was divided into two parts, one determined by the inlet fluid properties and the other being the pressure undershoot. Our experimental results show that the pressure undershoot and the liquid superheat at the incipient flashing location reach their maximum values with saturated inlet conditions; with increased inlet subcooling, thermal nonequilibrium decreased. A cavity nucleation model was developed for prediction of the pressure undershoot. The model includes a discharge coefficient, and it has been verified experimentally that this coefficient is a function of only the inlet liquid subcooling. Based on the present theory, the predicted critical mass flow rates are compared with not only our own experimental data but also other experimental data, and good agreement is achieved. © *Elsevier Science Inc., 1997*

Keywords: *convergent–divergent nozzle, critical flow, cavity nucleation model*

INTRODUCTION

For a light water nuclear reactor, the discharge rate from pressurized containers under the conditions of a loss-of-coolant accident (LOCA) determines the pressure decompression rate, the coolant level within the reactor vessel, and the design of the emergency core-cooling system (ECCS), etc. The discharge mass flow rate depends on the pressure, the temperature upstream of the break, and the break geometry, and a "choking" condition within the break geometry gives a maximum value. Early critical mass flow rate models such as the homogeneous equilibrium model and slip model cannot account for the effect of interface mechanical and thermal nonequilibrium, therefore poor agreement was obtained with these critical models. In recent years, the phenomenon of flashing flow has been studied in relation to the critical flow problem. Models that account for thermal nonequilibrium for initially subcooled or saturated states must represent the physics of the nucleation process and the growth of bubbles in a transient pressure environment. Ardron [1], Richter [2], Elias and Chambe [3], Dobran [4], and Shin and Jones [5] are some of the authors who have contributed detailed mechanistic models. These models require a great deal of information to complete the model description such as initial nucleation site density and bubble diameter, interphase friction characteristics and heat transfer, and criteria that account for different flow regimes.

Schrock et al. [6] examined the flashing phenomenon of initially subcooled water or nearly saturated water in convergent–divergent nozzles for inlet pressures less than 9.0 MPa. They developed a two-step model based on nucleation delay and discontinuous transition to two-phase flow followed by frozen composition. This model did not include the real physical behavior of the nucleation process, but they claimed that there was no satisfactory means of predicting the number and size of microbubbles in liquids. More recently, Lee and Schrock [7] developed a cavity flooding model to correlate the pressure undershoot data for constant-area pipe flow at ambient pressure.

Fincke [8] conducted critical flow experiments in short nozzles with subcooled inlet conditions in a low-pressure loop. He also developed a steam generation model based on heat transfer from a superheated liquid jet.

Abuaf et al. [9] examined experiments dealing with flashing flows in convergent–divergent nozzles and con-

Address correspondence to J. L. Xu, Institute of Nuclear Energy Technology, Tsinghua University, Beijing, 100084 People's Republic of China.

Experimental Thermal and Fluid Science 1997; 14:166–173

655 Avenue of the Americas, New York, NY 10010

0894-1777/97/$17.00
PII S0894-1777(96)00055-6

cluded that the incipient flashing always occurs at or very near the throat. The pressure undershoot at the throat is predicted by the Alamgir and Lienhard [10] correlation and considers the effect of turbulent intensity. However, the predicted mass flow rate has not been verified by experimental data.

In the present work, we carried out a transient critical flow experiment with a convergent–divergent nozzle as the break geometry for inlet pressure up to 16.0 MPa and measured the pressure distribution along the axial direction in detail. The concept of the incipient flashing point occurring at the throat was also applied in this work. From our experimental results, we know that the pressure undershoot at the throat is decreased when the inlet liquid subcooling is increased. An analytical theory based on the wall surface cavity nucleation process is presented to predict the pressure undershoot. The predicted critical mass flow rates were compared with experimental data and agreed within a standard deviation of 3.1%.

EXPERIMENT

A transient critical flow experiment was recently conducted at the high-pressure test loop of Xi'an Jiaotong University mainly to investigate the system's transition characteristics and measure the critical flow rate after a sudden break. As shown in Fig. 1, the feed water is pressurized by a plunger pump and separates into two circuits, one passing through the bypass to adjust the mass flow rate and the other flowing through orifices and a regenerative heat exchanger and then into a heated tube section with an inner diameter of 16.0 mm. The fluid out of the heated tube, which has controlled subcooling, enters the pressure vessel, which has a volume of about 0.125 m^3. The controlled subcooling water exits the bottom of pressure vessel through a tube with an inner diameter of 30.0 mm. The break section, also shown in Fig. 1, mainly consists of the break nozzle and a shutoff gate valve. When the main circuit is operated under the conditions of a controlled system pressure with a controlled flow rate and subcooling of the fluid entering the pressure vessel, the shutoff gate valve is opened suddenly, and the total time for the gate valve from fully closed to fully open is less than 0.5 s. The hot water then discharges through the break nozzle, enters a short expansion tube with an inner diameter of 20.0 mm, and is collected in a catch tank. In order to cool the discharge two-phase mixture, a coiled copper heat exchanger is inserted in the catch tank. The catch tank is supported vertically on two lugs through the two load cells. By use of the two load cells, the time-dependent mass of the catch tank can be measured, from which we can acquire the discharge flow rate through the break nozzle.

Initially, by adjusting valves A and B, the desired system pressure P_0 and main circuit flow rate G_0 can be obtained. By adjusting the alternating current power supplied at the heating tube at the given mass flow rate, we can obtain the desired subcooling, ΔT_{sub}, of the fluid entering the pressure vessel. Under the conditions of steady operation, the shutoff gate valve is opened suddenly.

The mass flow rate of the main circuit is measured at two orifices before the fluid enters the regenerative heat exchanger. The fluid temperatures are measured by the NiCr-NiSi jacket thermocouples along the heated tube at the inlet and outlet of the pressure vessel. The differential pressure transducer is installed between the top and bottom of the pressure vessel to determine the liquid level during the discharge period. The pressure gauges are set along the nozzle axial length, upstream and downstream of the nozzle. Fluid temperatures upstream and downstream of the nozzle are also measured by NiCr-NiSi jacket thermocouples. The uncertainties of the pressures and temperatures are ± 0.05 MPa (maximum relative error of 1.6%) and ± 1°C, respectively, while the error of the discharge mass measurement is within ± 0.98%. All

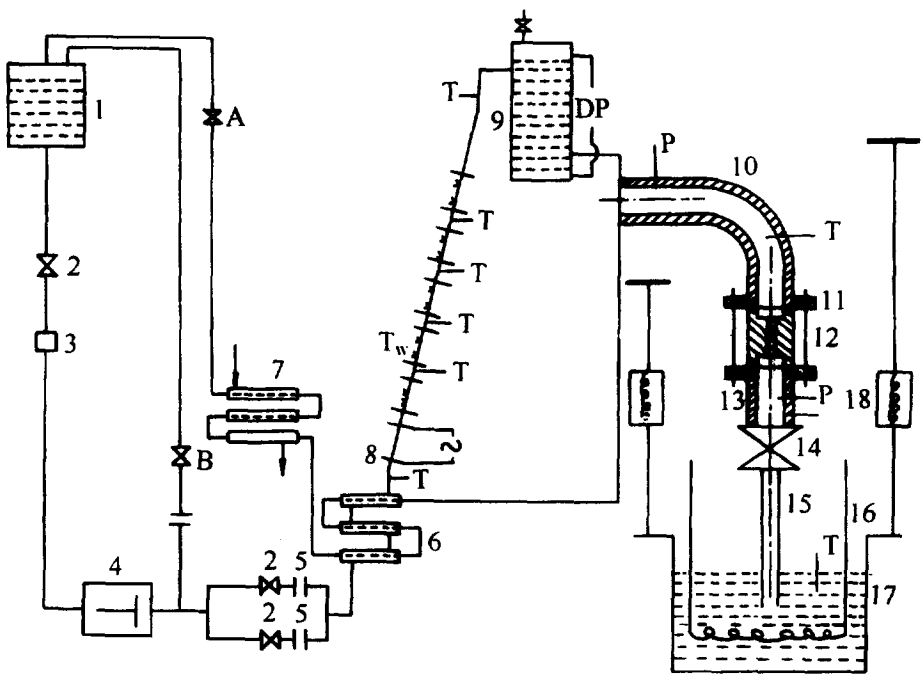

Figure 1. Transient critical flow experiment system. *1*, Water tank; *2*, control valve; *3*, filter; *4*, high-pressure plunger pump; *5*, orifice; *6*, regenerative heat exchanger; *7*, heat exchanger; *8*, electrode; *9*, pressure vessel; *10*, connection tube upstream of the break nozzle; *11*, flange; *12*, break nozzle; *13*, connection tube downstream of the break nozzle; *14*, shutoff gate valve; *15*, expansion section; *16*, coiled copper heat exchanger; *17*, water catch tank; *18*, load cell. *P*, pressure gauge; *T*, fluid temperature gauge; T_w, wall temperature gauge; DP, differential pressure transducer.

electric signals are transferred to an IBM 386 computer through an IMP 3595C high quality data collector (England).

Conceptually, the tank mass inventory method is the simplest. In this approach, the tank mass measurements obtained from two load cells are differentiated with respect to time. This yields the mass flow rate directly. The slope of the resulting best fit line is taken to be the mass flow rate. This method depends on the assumption that the flow is quasi-static. For time of less than 1–2 s after the gate valve opening at the very early stage of discharge, this method may introduce an error into the mass flow rate, the maximum error estimated to be 6% in this short period. After this early discharge period, the mass flow rate error is estimated to be 0.98%. Typical pressure, temperature, integrated discharge mass, and corresponding mass flow rate transients are shown in Fig. 2.

The nozzle geometry and dimensions are shown in Fig. 3. The constant-area tube diameter upstream of the convergent section is 30.0 mm, the throat diameter is 4.18 mm (measured by optical microscope), and the expansion tube diameter followed by the divergent section is 25.4 mm. The half-angles of the convergent and divergent sections are 30° and 12°, respectively.

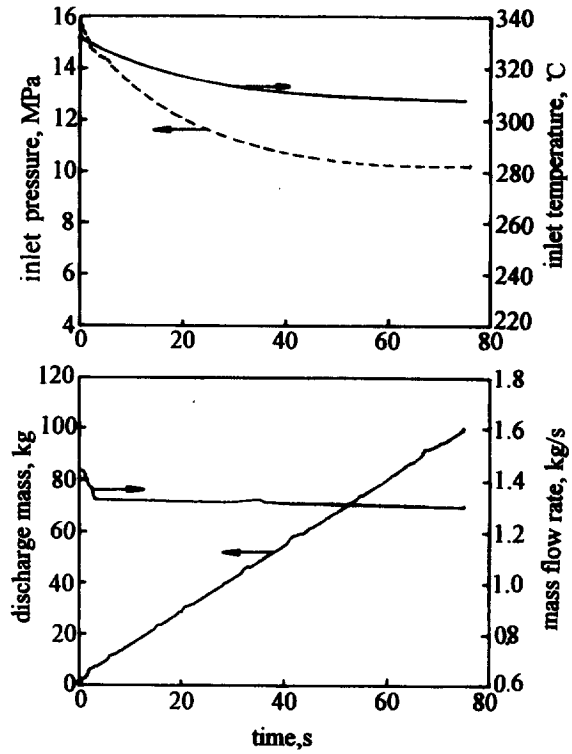

Figure 2. Typical pressure, temperature, discharge mass, and mass flow rate transients.

When the inlet subcooled liquid $[P_0, T_0;\ T_0 \le T_{sat}(P_0)]$ enters the nozzle, it should travel a distance z_i to reach the pressure $P_{sat}(T_0)$; further flowing causes the fluid pressure to decrease to the throat pressure P_t. If we assume that at the incipient flashing, the choking plane occurs at the throat section, then $\Delta P_2 = P_{sat}(T_0) - P_t$ is the so-called pressure undershoot. The corresponding liquid superheat is $T_0 - T_{sat}(P_t)$. Both the pressure undershoot and the liquid superheat describe the thermal nonequilibrium as the incipient flashing occurs. Therefore the total pressure difference $P_0 - P_t$ consists of two parts:

$$P_0 - P_t = [P_0 - P_{sat}(T_0)] + [P_{sat}(T_0) - P_t]$$
$$= \Delta P_1 + \Delta P_2. \quad (1)$$

It is apparent that ΔP_1 is determined only by the inlet stagnation properties of (P_0, T_0).

The critical mass flow rate can be written as follows by applying the single-phase Bernoulli equation in the convergent section:

$$G = \sqrt{2\rho_L(P_0 - P_t)}, \quad (2)$$

where ρ_L is the liquid density. So the problem of obtaining the critical mass flow rate lies in predicting the throat pressure P_t or the pressure undershoot ΔP_2. With inlet saturated liquid entering the nozzle, the liquid becomes superheated shortly after it enters the convergent section of the nozzle, because $\Delta P_1 = 0$, and the critical mass flow rate is determined only by the square root of the pressure undershoot.

From our experimental results, we know that the critical mass flow rates are increased with increasing inlet stagnation pressure as the inlet saturated liquid discharges. The critical mass flow rates also increase as the inlet liquid subcooling increases at a given inlet pressure. The larger critical mass flow rate is produced not only by the pressure undershoot but also by ΔP_1, which is determined by the inlet stagnation liquid properties. Another important phenomenon is that the pressure undershoot is decreased with increasing inlet liquid subcooling, as shown in Fig. 4. Therefore we may infer that the fluid is very close to the saturated state at the incipient flashing under the condition of very high inlet liquid subcooling, the pressure

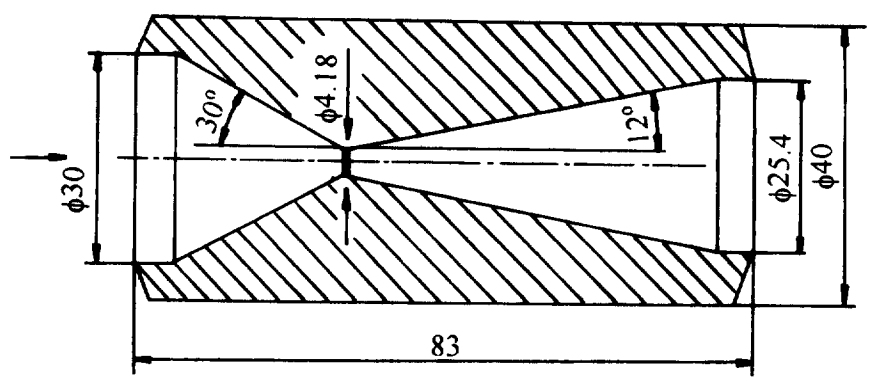

Figure 3. Convergent–divergent nozzle geometry and dimensions (all dimensions are in mm).

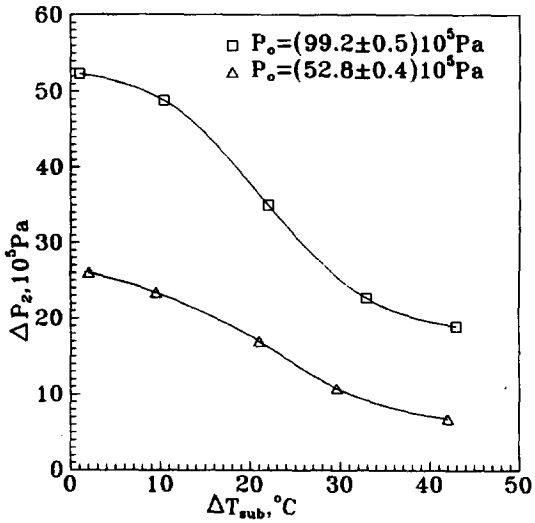

Figure 4. Pressure undershoot at incipient flashing versus inlet liquid subcooling.

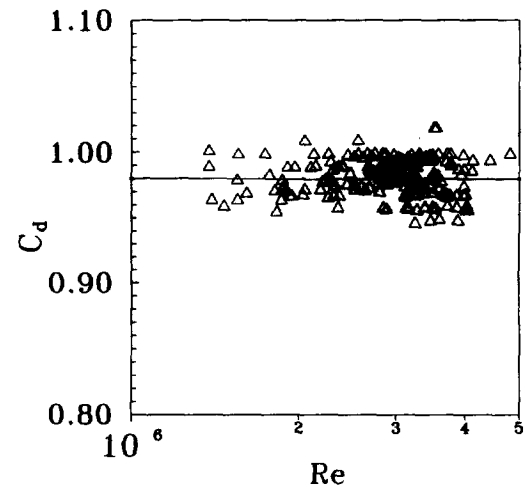

Figure 5. Discharge coefficient versus throat Reynolds number.

undershoot and the liquid superheat are small, and the higher critical mass flow rate is mainly contributed by the square root of ΔP_1.

It may be noted that a discharge coefficient C_d should be introduced to consider the effect of the nozzle geometry, etc. C_d is defined by

$$C_d = \frac{G}{[2\rho_L(\Delta P_1 + \Delta P_2)]^{1/2}}, \tag{3}$$

where G is the measured mass flow rate mentioned above and ΔP_2 is obtained by measuring the pressure P_t at the incipient flashing location. Values of C_d are plotted in Fig. 5 for liquid Reynolds numbers covering the range of 1×10^6–5×10^6. It is shown that C_d is very close to unity, indicating that fluid jet separation does not occur. Early investigations suggested that C_d is nearly equal to 0.64 with liquid flowing in sharp-edged tubes; under this condition, the fluid should travel some distance to fill the pipe at the pipe entrance region. Based on Fig. 5, we set $C_d = 0.98$ in the present work.

Typical experimental results are listed in Table 1.

WALL SURFACE CAVITY NUCLEATION MODEL

Alamgir and Lienhard [10] developed a semiempirical correlation for prediction of the pressure undershoot based on static decompression data. They applied homogeneous nucleation theory, modified to account for the smaller amount of work needed to produce a spherical nucleus on the bounding wall. Such a nucleus is created by the inherent molecular energy fluctuations in the superheated liquid state. Little work has been done to examine the flashing delay in a flowing decompression system.

Xu and Chen [11] pointed out that the high liquid velocity in a high-velocity flow decompression system may depress the incipient flashing process occurring in the liquid or the mixture; that is to say, the incipient flashing process appears mainly on the wall surface. Therefore it is proposed that incipient boiling is governed by wall surface cavity nucleation. A similar model was applied by Lee and Schrock [7] to predict the critical flow for a constant-area pipe at low pressures. Liquid superheat is caused by the decreasing pressure in the isothermal single-phase flow. When the liquid superheat or the pressure undershoot reaches a certain value, the wall surface begins to produce nucleation cavities. The present problem is similar to that of nucleate boiling except that superheating is caused by depressurization rather than by heating.

Fabic [12] investigated the nucleation process on a wall surface subjected to transient heating. Heating causes a vapor pressure rise in the cavities, and further heating makes the superheated liquid move out of the cavities due to the increase in the vapor pressure. Shin and Jones [5] also developed a cavity nucleation model, but their analysis was mainly concerned with the nucleation frequency rather than the incipient flashing.

A more realistic cavity is assumed in Fig. 6. The vapor pressure in the cavity is $P_{sat}(T_0)$, and when the subcooled liquid at the state (P_0, T_0) advances into the cavity, a liquid/vapor interface is formed as shown in Fig. 6*a*. The force balance equation across such an interface can be written as

$$P_0 - P_{sat}(T_0) = \frac{2\sigma(T_0)}{R_1}, \tag{4}$$

where R_1 is the curvature radius of the meniscus and $\sigma(T_0)$ is the surface tension at a temperature of T_0.

It should be noted that there exists an advancing contact angle $\beta_0 > 90°$ for supporting the pressure difference across the vapor/liquid interface. The cavity radius is

$$r_c = R_1 \cos(\pi - \beta_a + 0.5\theta). \tag{5}$$

Now our attention is directed to the superheated liquid receding from the cavity as shown in Fig. 6*b*; the state of the superheated liquid is (P_t, T_0). The force balance equation across the vapor/liquid interface at this condition is

$$P_{sat}(T_0) - P_t = \frac{2\sigma(T_0)}{R_2}. \tag{6}$$

Table 1. Typical Experimental Data for Critical Flow in a Nozzle

P_0 (MPa)	T_0 (°C)	ΔT_{sub} (°C)	P_t (MPa)	$P_0 - P_{sat}(T_0)$ (MPa)	$P_{sat}(T_0) - P_t$ (MPa)	ΔT_{sup} (°C)	G [10^3 kg / (m^2 s)]
2.96	216.3	16.7	1.45	0.80	0.71	19.71	50.51
3.89	243.1	5.6	1.86	0.36	1.67	34.3	57.33
4.20	249.4	3.8	1.98	0.26	1.95	37.4	59.52
5.06	262.1	2.5	2.34	0.20	2.52	41.7	65.16
5.79	271.5	1.8	2.53	0.16	3.10	46.9	70.68
4.90	256.8	5.8	2.20	0.44	2.26	39.7	65.29
4.64	239.4	19.9	2.07	1.33	1.24	25.2	64.71
4.10	238.2	13.6	1.92	0.86	1.33	28.0	59.69
5.97	265.0	10.2	2.45	0.88	2.64	42.2	73.99
6.75	276.7	6.7	2.68	0.65	3.42	48.9	78.52
7.57	290.1	1.0	3.13	0.11	4.32	53.9	80.57
5.99	255.1	20.3	2.43	1.66	1.90	32.7	75.16
6.55	272.5	8.9	2.60	0.83	3.11	46.3	77.73
7.48	282.6	7.7	2.89	0.80	3.78	50.7	83.75
8.27	292.5	4.8	3.24	0.55	4.48	54.3	85.62
8.54	266.9	32.7	2.94	3.30	2.30	34.2	93.36
6.84	275.8	8.5	2.73	0.82	3.29	47.2	79.04
6.32	272.1	6.8	2.67	0.63	3.02	44.6	74.66
7.35	286.4	2.7	3.07	0.29	4.00	51.4	79.58
8.70	299.7	1.2	3.56	0.14	5.00	56.2	85.66
10.90	315.9	1.5	4.61	0.22	6.08	57.0	92.36
9.96	277.8	32.9	3.93	3.75	2.27	28.4	95.70
7.42	285.8	4.0	3.80	0.42	3.18	38.1	73.01
8.72	299.3	1.8	3.56	0.21	4.95	55.8	85.86
10.31	307.5	5.7	3.92	0.78	5.61	58.3	94.46
7.62	272.4	19.2	2.83	1.91	2.88	41.8	85.70
7.40	276.2	13.3	2.78	1.34	3.28	46.6	83.77
7.63	287.6	4.1	3.09	0.44	4.10	52.2	81.84
9.13	297.0	7.4	3.37	0.90	4.86	56.6	91.08
9.14	297.1	7.4	3.40	0.90	4.84	56.1	90.92
8.08	284.2	11.4	3.03	1.24	3.81	49.8	86.37
9.48	306.1	0.9	5.74	0.12	3.62	33.4	72.29
9.85	309.0	0.8	4.92	0.11	4.82	46.2	82.68
9.32	301.8	4.0	3.74	0.50	5.08	55.5	89.00
9.82	308.5	1.1	4.03	0.15	5.64	57.7	89.63
10.71	309.5	6.6	3.92	0.91	5.88	60.3	97.08
10.26	307.3	5.5	3.85	0.75	5.66	59.2	94.60
11.60	317.6	10.4	10.66	0.66	6.28	58.1	96.79
11.49	316.6	4.7	4.50	0.69	6.30	59.3	97.34
13.21	328.4	3.7	6.35	0.60	6.26	49.2	94.28
12.90	328.1	2.1	6.31	0.35	6.25	49.3	92.40
11.56	316.5	5.3	4.49	0.79	6.28	59.2	97.90
12.93	326.4	4.0	5.83	0.65	6.45	52.7	96.27
13.84	305.9	29.9	4.27	4.52	5.05	51.6	116.61
9.87	297.5	12.5	3.60	1.58	4.70	53.4	95.08
10.86	316.3	0.9	4.50	0.13	6.22	58.7	92.79
10.01	294.8	16.2	3.57	2.03	4.41	51.1	96.75
11.59	318.2	3.7	5.20	0.56	5.83	51.9	92.72
11.48	320.1	1.2	5.19	0.18	6.11	53.8	91.63
15.65	313.5	32.0	4.80	5.30	5.55	52.1	122.95
13.13	321.3	10.3	5.07	1.64	6.42	56.5	103.87
11.64	321.5	0.9	5.24	0.13	6.27	54.6	92.23
10.66	295.4	20.2	3.68	2.61	4.37	50.0	100.68
13.76	330.6	4.7	6.96	0.80	6.00	45.2	93.48
14.54	334.1	5.6	7.96	0.98	5.60	39.5	91.35

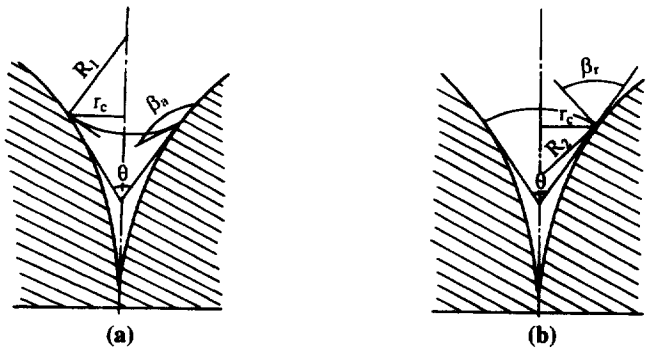

Figure 6. (*a*) Subcooled liquid advancing into the cavity. $r_c = R_1 \cos(\pi - \beta_a + 0.5\theta)$. (*b*) Superheated liquid receding from the cavity. $r_c = R_2 \cos(\beta_r + 0.5\theta)$.

When the meniscus begins to move out of the cavity, the receding angle β_r reaches a value of less than 90° ($\beta_r < 90°$), and the cavity radius is

$$r_c = R_2 \cos(\beta_r - 0.5\theta). \tag{7}$$

Combining Eqs. (4)–(7) gives the expression

$$\frac{\cos(\pi - \beta_a)\cos(0.5\theta) - \sin(\pi - \beta_a)\sin(0.5\theta)}{\cos\beta_r \cos(0.5\theta) + \sin\beta_r \sin(0.5\theta)} = \frac{P_0 - P_{sat}(T_0)}{P_{sat}(T_0) - P_t}, \tag{8}$$

where $P_0 - P_{sat}(T_0)$ and $P_{sat}(T_0) - P_t$ are respectively ΔP_1 and ΔP_2, which were defined in the preceding section. We specify that $c = \Delta P_1/\Delta P_2$; thus the conical contact angle at the meniscus is expressed as

$$\theta = 2\arctan\left[\frac{\cos(\pi - \beta_a) - c\cos\beta_r}{\sin(\pi - \beta_a) + c\sin\beta_r}\right]. \tag{9}$$

For a given inlet stagnation state (P_0, T_0), $c = \Delta P_1/\Delta P_2$ assumes a certain value. Equation (9) illustrates the relation of the conical contact angle θ to c.

On the basis of experimental data for water and stainless steel, Fabic [12] suggested that $\beta_a = 109°$ and $\beta_r = 80°$, and these values were also applied in the present analysis. Particularly, with saturated inlet stagnation conditions, $c = \Delta P_1/\Delta P_2 = 0$; thus we obtain $\theta = 38°$ by use of Eq. (9). With increased inlet stagnation subcooling, ΔP_1 is increased and ΔP_2 is decreased, which implies that c reaches a high value that eventually decreases the conical contact angle θ.

CRITICAL FLOW WITH SATURATED INLET CONDITIONS

$\bar{R}_2$ is defined as the radius of curvature of the meniscus at the liquid/vapor interface when the wall surface cavity begins to nucleate for saturated inlet stagnation conditions. By use of Eq. (6), $\bar{R}_2$ is predicted as

$$\bar{R}_2 = \frac{2\sigma(T_0)}{\Delta P_{2,exp}}. \tag{10}$$

When ΔP_2 is determined by experimentation, the surface tension is represented by

$$\sigma = 0.2358(1 - T_r)^{1.256}[1 - 0.625(1 - T_r)], \tag{11}$$

where T_r is the reduced temperature $T_r = (T_0 + 273.15)/647.27$.

It is apparent that $\bar{R}_2$ is determined only by the inlet stagnation pressure P_0. With P_0 covering the range of 3.0–16.0 MPa in the present experiment, $\bar{R}_2$ is correlated as

$$\bar{R}_2 = 2.13062 \times 10^6 P_0^{-2.09466}, \tag{12}$$

where P_0 is in pascals. A curve of $\bar{R}_2$ versus P_0 is illustrated in Fig. 7.

CRITICAL FLOW WITH SUBCOOLED LIQUID INLET CONDITIONS

As discussed above, the pressure undershoot and the liquid superheat at the flash incipient location decrease as the inlet stagnation liquid subcooling increases. Therefore, based on Eq. (6), the radius of curvature of the meniscus at the liquid/vapor interface increases as ΔT_{sub} increases. Here we introduce a coefficient that is defined as the ratio of the curvature radius of the meniscus with subcooled liquid inlet conditions to that with saturated inlet conditions at the same pressure.

$$\eta = \frac{R_2}{\bar{R}_2} \tag{13}$$

where $R_2 = 2\sigma(T_0)/\Delta P_{2,exp}$, $\Delta P_{2,exp}$ is the experimental pressure undershoot at the incipient flash point with subcooled inlet conditions and $\bar{R}_2$ is predicted from Eq. (12). It is found that η is a function of only inlet subcooling. This dependence is verified by plotting experimentally obtained values of η versus subcooling (see Fig. 8). Such a relation can also be explained as that for different inlet stagnation pressure, η is same for a given inlet subcooling. The correlation is found as

$$\eta = 0.804068 \exp(0.01440201\,\Delta T_{sub}). \tag{14}$$

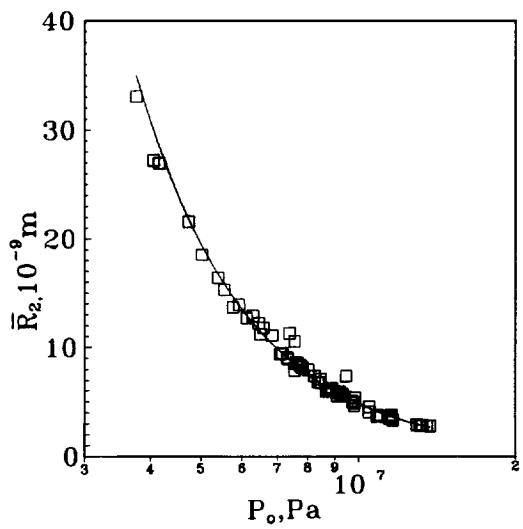

Figure 7. Correlation of R_2 with inlet pressure.

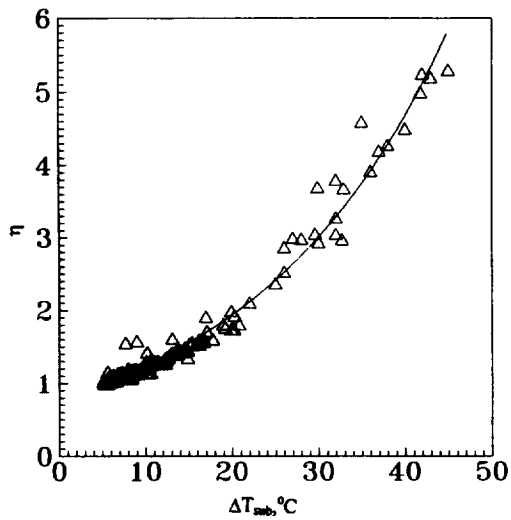

Figure 8. Correlation of η with inlet liquid subcooling.

RESULTS AND DISCUSSION

By use of the present wall surface cavity nucleation theory, Eqs. (12) and (14) are experimentally correlated over a wide range of parameters. For a given inlet stagnation state (P_0, T_0), $\overline{R}_2$ and η are determined from Eqs. (12) and (14), respectively. Then the radius of curvature of the meniscus is acquired; thus we obtain the value of the pressure undershoot. Figure 9 shows a comparison of experimental critical mass flow rates and predicted values (standard deviation of 3.1%).

Schrock et al. [6] published the critical mass flow rates of initially nearly saturated or subcooled water discharging through nozzles for stagnation pressures P_0 = 0.794–9.05 MPa and temperatures of 23.3–286.7°C. Two kinds of nozzles were used, with throat diameters of 6.4 mm for the No. 2 nozzle and 3.96 mm for the No. 3 nozzle. All nozzles had half-angles of 40° in the convergent section and 12° in the divergent section, and the exit diameters of the divergent section were 31.8 mm for the No. 2 nozzle and 25.60 mm for the No. 3 nozzle.

The new theory predictions are compared with experimental data collected by Schrock et al. [6] in Fig. 10. It is seen that they match well, even though Eqs. (12) and (14) were developed with only our own experimental data.

From these comparisons, we see that the present correlations cover a wide range of inlet pressures and temperatures and they are suitable for convergent–divergent nozzles with half-angles of 30–40° in the convergent section.

PRACTICAL SIGNIFICANCE AND USEFULNESS

Since the Three-Mile Island accident, great attention has been paid to small-break loss-of-coolant accidents for typical commercial pressurized water reactors. When a small break occurs, it is important to determine the discharge mass flow rate, as this loss mass flow rate is very helpful in the design of an emergency core-cooling system. For instance, during the early stages of break discharge, the discharge mass flow rate should be carefully estimated to determine the injection water flow rate from the high-pressure injection system. The discharge mass flow rate depends not only on the upstream fluid properties but also on the break size and geometry. However, it is difficult to specify the break geometry, among the different break geometries such as sharp-edged tube, radius entry constant-area pipe, orifice, and convergent–divergent nozzles, the loss mass flow rate of liquid discharging through a convergent–divergent nozzle attains maximum values at the same break diameter and upstream conditions.

In the present paper, detailed experimental data have been described that were acquired for small-break loss-of-coolant accidents of a typical commercial pressurized water reactor, and a new simple model was developed to

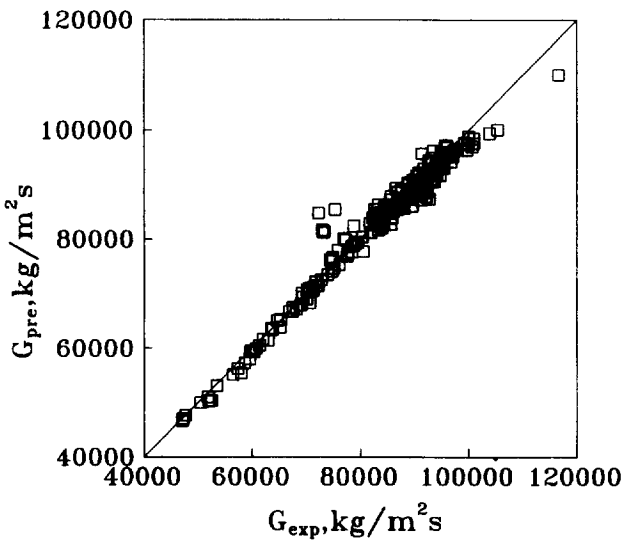

Figure 9. Comparison of the predicted critical mass flow rates with our own experimental data.

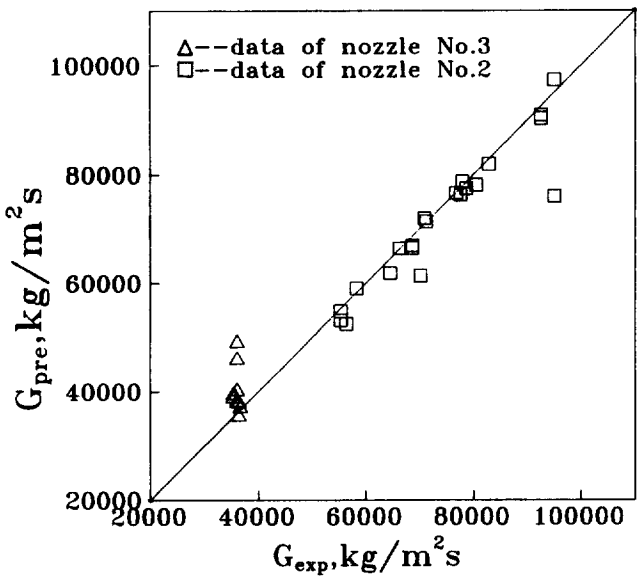

Figure 10. Comparison of the predicted critical mass flow rates with the data of Schrock et al. [6].

correlate the mass flow rate. The new correlations are also useful for estimating the mass flow rate of liquid discharging from other high-pressure containers.

CONCLUSIONS

1. A transient critical flow experiment was conducted for inlet stagnation pressures P_0 = 3.0–16.0 MPa and initial liquid subcooling ΔT_{sub} = 0–60°C.
2. Experimental results show that with increased inlet subcooling, the critical mass flow rates are increased; however, the pressure undershoot and liquid superheat at incipient flashing are decreased.
3. When the incipient flashing and the choking plane are assumed to occur at the throat location, the problem of predicting the critical mass flow rate is to determine the pressure undershoot.
4. A new wall surface cavity nucleation model is presented. Based on this theory, the conical contact angle at the meniscus of the nucleation cavity θ is 38° when saturated liquid initially discharges through the nozzles. With increased inlet stagnation subcooling, the conical contact angle at the meniscus (θ) is decreased while the curvature radius of the meniscus is increased.
5. The predicted mass flow rates based on the new wall surface cavity nucleation model match not only our own experimental data but also those of Schrock et al. [6] very well even though Eqs. (12) and (14) are based only on our own experimental data.
6. The present correlations are suitable for convergent–divergent nozzles at half-angles of 30–40° in the convergent section.

We are grateful for the financial support of the National Natural Science Foundation of China.

NOMENCLATURE

c defined as $\Delta P_1/\Delta P_2$, dimensionless
C_d discharge coefficient, dimensionless
G critical mass flow rate, kg/(m^2 s)
P_0 inlet pressure, Pa
$P_{sat}(T_0)$ saturated pressure at temperature T_0, Pa
P_t pressure at throat location, Pa
r_c cavity radius, m
R_1 radius of curvature of the meniscus for subcooled liquid advancing into the cavity, m
R_2 radius of curvature of the meniscus for superheated vapor receding from the cavity, m
$\overline{R_2}$ radius of curvature of the meniscus for superheated vapor receding from the cavity at saturated liquid inlet conditions, m
T_0 inlet temperature, °C
T_r reduced temperature, °C

Greek Symbols

β_a advancing contact angle, deg
β_r receding angle, deg
ΔP_1 $P_0 - P_{sat}(T_0)$, Pa
ΔP_2 pressure undershoot, Pa
ΔT_{sub} inlet liquid subcooling, °C
ΔT_{sup} liquid superheating, °C
η defined as in Eq. (13), dimensionless
θ conical contact angle, deg
ρ_L liquid density, kg/m^3
σ surface tension, N/m

REFERENCES

1. Ardron, K. H., A Two-Fluid Model for Critical Vapor–Liquid Flow, *Int. J. Multiphase Flow* **4**(3), 327–337, 1978.
2. Richter, H. J., Separated Two-Phase Flow Model: Application to Critical Two-Phase Flow, *Int. J. Multiphase Flow* **9**(5), 511–530, 1983.
3. Elias, E., and Chambe, P. L., A Mechanistic Nonequilibrium Model for Two-Phase Critical Flow, *Int. J. Multiphase Flow*, **10**(1), 21–40, 1984.
4. Dobran, F., Nonequilibrium Modeling of Two-Phase Critical Flows in Tubes, *ASME J. Heat Transfer* **109**, 731–738, 1987.
5. Shin, T. S., and Jones, O. C., Jr., An Active Cavity Model for Flashing, *Nucl. Eng. Design* **95**, 185–196, 1986.
6. Schrock, V. E., Starkman, E. S., and Brown, R. A., Flashing Flow of Initially Subcooled Water in Convergent–Divergent Nozzles, *ASME J. Heat Transfer* **99**, 263–268, 1977.
7. Lee, S. Y., and Schrock, V. E., Critical Two-Phase Flow in Pipes for Subcooled Stagnation States with a Cavity Flooding Incipient Flashing Model, *ASME J. Heat Transfer* **112**, 1032–1039, 1990.
8. Fincke, J. R., The Correlation of Nonequilibrium Effects with Choked Nozzle Flow with Subcooled Upstream Conditions, Conference Paper, ANS Small Break Specialist Meeting, California, pp. 1–30, 1981.
9. Abuaf, N., Jones, O. C., Jr., and Wu, B. J. C., Critical Flashing Flows in Nozzles with Subcooled Inlet Conditions, *ASME J. Heat Transfer* **105**, 379–383, 1983.
10. Alamgir, M. D., and Lienhard, J. H., Correlation of Pressure Undershoot During Hot Water Depressurization, *ASME J. Heat Transfer* **103**, 52–55, 1981.
11. Xu, J. L., and Chen, T. K., Two-Phase Critical Flow, *Chin. J. Adv. Mech.* **25**(1), 77–84, 1995.
12. Fabic, S., Vapour Nucleation of Surfaces Subjected to Transient Heating, Ph.D. Thesis, Univ. California, Berkeley, 1964.

Received October 20, 1995; revised April 15, 1996